Applied Catalysis B: Environmental 140–141 (2013) 51–59

Contents lists available at SciVerse ScienceDirect

Applied Catalysis B: Environmental

journal homepage: www.elsevier.com/locate/apcatb

Effect of Sn surface states on the photocatalytic activity of anatase TiO_2

Freddy E. Oropeza, Bastian Mei, Ilia Sinev, Ahmet E. Becerikli, Martin Muhler, Jennifer Strunk*

Laboratory of Industrial Chemistry, Ruhr-University Bochum, Universitätsstrasse 150, 44801 Bochum, Germany

ARTICLE INFO

Article history:
Received 12 November 2012
Received in revised form 22 March 2013
Accepted 27 March 2013
Available online 2 April 2013

Keywords:
Photocatalysis
TiO_2
SnO_2
Dye degradation
Grafting
Surface doping
Temperature-programmed reduction
X-ray absorption spectroscopy
X-ray photoelectron spectroscopy
Surface charge trapping

ABSTRACT

The influence of surface Sn-doping on the photocatalytic properties of anatase TiO_2 has been investigated in samples prepared by a grafting route using Sn(IV) *tert*-butoxide as Sn precursor. The grafting procedure leads to the formation of isolated Sn(IV) sites on the surface of anatase TiO_2 powders as gauged by structural characterisation based on XRD, Raman spectroscopy and XAS. Studies of the surface reduction based on TPR experiments and XPS provide the conditions for a selective reduction of surface Sn(IV) to the divalent oxidation state. Electronic structure characterisation based on valence band XPS and DRS shows that there is a slight widening of the band gap upon Sn(IV)-grafting, but Sn(II) related states emerge at the top of the main valence band upon reduction at temperatures up to 350 °C, and this induces visible light absorption. Grafting of TiO_2 with Sn(IV) increases the formation rate of •OH radicals on the surface of the material. Reduction of the Sn(IV)-grafted TiO_2 to form surface Sn(II) brings about substantial increase of the photocatalytic efficiency for the methylene blue degradation under irradiation with $\lambda \geq 320$ nm compared with Sn(IV)-grafted and pure anatase TiO_2. This observation is explained based on a surface hole trapping by the Sn(II)-related surface states which lie above the top of the main valence band and can therefore act as trapping sites for holes produced under photoexcitation.

1. Introduction

There is a growing interest in the use of wide band-gap oxide semiconductors as photocatalysts with the ability to use sunlight to bring about reactions such as the degradation of organic pollutants or the production of hydrogen from water or hydrocarbons. TiO_2 and SnO_2 are both well characterised semiconductors that have been shown to act as photocatalysts for some of those important reactions. Furthermore, being of great abundance and low price, these materials are very attractive for industrial application. However, the use of these solids in solar energy technologies is limited because they are *only active under UV irradiation*, which represent less than 5% of the solar spectrum. A second factor that limits the activity of photocatalysts, and therefore their applied use, is *the quick recombination of the electrons and holes generated under irradiation*.

Visible light photocatalytic activity has been previously achieved by cationic and anionic doping of TiO_2 with coloured transition metals [1] and with nitrogen [2,3], respectively. Nonetheless, this method often decreases the catalytic efficiency of TiO_2 by inhibiting charge migration through the metal oxide [1,4] because of carrier localisation produced by the breaking of translational symmetry upon the positionally disordered introduction of dopant species [5]. However, it has been reported that low level doping of TiO_2 with Sn(IV) enhances its photocatalytic activity towards the oxidation of organic compounds under visible light [6,7] as well as in UV light [8–10].

SnO_2 has the rutile TiO_2 structure and it is possible to prepare rutile solid solutions in the whole range of concentrations [11,12]. Anatase TiO_2 with up to 10% Sn doping has been also successfully synthesised [13]. Regardless of the polymorph, Sn-doping in TiO_2 leads to an enhanced photocatalytic activity, especially in the range 0–10% of Sn cation contents [13,14]. Based on electronic structure studies of rutile $Sn_xTi_{1-x}O_2$ solid solutions, the improved photocatalytic activity upon Sn doping has been partially attributed to surface states associated with segregated Sn ions in the divalent state. Free post-transitional metal ions in the $N-2$ oxidation state such as Sn^{2+} and Sb^{3+} have a configuration $5s^25p^0$. In solid state oxides, the 5s electrons hybridise strongly with O 2p states to give antibonding states of mixed metal 5s–O 2p character at the top of the valence band. These states can further interact with nominally empty metal 5p states to give a directional electron lone pair as long as the cation occupies a site which lacks inversion symmetry [15–17]. Bulk sites within the rutile structure are centrosymmetric, but the lowered coordination at surface sites removes the inversion symmetry, which allows the 5s–5p hybridisation and a lowering

* Corresponding author. Tel.: +49 2343223566.
E-mail address: jennifer@techem.rub.de (J. Strunk).

0926-3373/$ – see front matter © 2013 Elsevier B.V. All rights reserved.
http://dx.doi.org/10.1016/j.apcatb.2013.03.043

of the internal electronic energy of the dopant ion. Thus segregation and reduction of bulk ions in the *N* oxidation state to give surface ions in the $N-2$ oxidation state lowers the surface energy and provides a thermodynamic driving force for segregation. Since Sn(II)-derived electronic states lie above the top of the main valence band of TiO_2, they induce visible light absorption and act as trapping sites for holes produced under photoexcitation [18,19].

The effect of bulk Sn(II)-doping in TiO_2 has been recently studied by Boppana and Lobo [20]. Although no clear evidence of tin incorporation into the TiO_2 lattice was provided, it was found that Sn(II)-doped samples were active towards the photocatalytic oxidation of organic compounds under visible light irradiation ($\lambda > 420$ nm). However, photocatalytic tests using the full range of a Xe lamp (UV–vis light) showed that pure TiO_2 was more active than doped samples. Moreover, within the range of concentrations studied, higher concentrations of tin led to a further decrease of the photocatalytic efficiency of the solid.

Here, we report a study of the effect of Sn(II)-doping of TiO_2 restricted to the surface. Surface Sn(II)-doped TiO_2 samples were prepared by a controlled reduction of Sn(IV)-grafted anatase TiO_2, based on combined analysis of temperature programmed reduction (TPR) profiles and X-ray photoelectron spectra (XPS). Photocatalytic characterisation based on methylene blue degradation and terephthalic acid hydroxylation shows that surface Sn(II)-doping greatly enhances the activity and overall efficiency of TiO_2 in degradation of organics. Enhanced photocatalytic efficiency can be attributed to the larger concentration of oxidising agents at the surface of the material as Sn(II) surfaces states act as hole trapper sites.

2. Experimental

2.1. Preparation of samples

The procedure used for grafting tin onto commercial anatase TiO_2 was based on the deposition of TiO_x on MCM-48 as previously reported [21]. With the help of a glove box and a vacuum line the procedure here described was carried out under inert atmosphere. Approximately 2 g of TiO_2 (pure anatase with 100 m^2/g supplied by Sachtleben) were dried over night at 120 °C under dynamic vacuum. The Sn precursor, tin (IV) *tert*-butoxide (Aldrich, 99.99%) was dissolved in about 50 ml of dry toluene. The amount was chosen according to the desired surface coverage, with maximum of 1.5 Sn/nm^2. The precursor solution was brought in contact with the dry support at room temperature and stirred for at least 4 h. The support was separated from the solution by means of sedimentation. The Sn-grafted TiO_2 was then was washed three times with dry toluene (~30 ml), separating sample and solution each time by sedimentation, and dried under dynamic vacuum. The calcination was performed by heating the sample with 2 °C/min under a flow of 100 ml/min N_2 to 300 °C holding the temperature for 1 h. During the time at 300 °C, the gas flow was switched to synthetic air, before the temperature was ramped at 2 °C/min to 450 °C and kept for 4 h. Grafted samples were labelled as Sn(*x*)/TiO_2, where x is the nominal Sn loading in atoms of tin per nm^2.

2.2. Physicochemical characterisation

Powder X-ray diffraction (XRD) and Raman spectroscopy were used to check crystalline phase of the samples. XRD was carried out on a Panalytical X'Pert Pro instrument using monochromated Cu $K\alpha_1$ radiation, whereas Raman spectra were recorded at room temperature using a Thermo Fisher Scientific FT-Raman spectrometer with excitation by a Nd:YAG laser ($\lambda = 1064$ nm).

Reduction of the samples was studied by temperature-programmed reduction (TPR). All TPR profiles were taken in a flow setup using 4.54% H_2 in argon at a rate of 84.1 ml/min. The reactor was heated from room temperature to 850 °C at a rate of 5 °C/min and held for 60 min. The H_2 concentration in the gas flow was analysed by thermal conductivity detector.

Electronic characterisation was based on valence band photoemission spectroscopy and UV/vis diffuse reflectance spectroscopy. X-ray photoemission spectra (XPS) were recorded on a UHV system equipped with a Gammadata-Scienta SES 2002 analyzer. The base pressure in the measurement chamber was 5×10^{-10} mbar. Monochromatic Al Ka (1486.6 eV; 13.5 kV; 37 mA) was used as incident radiation and the analyzer pass energy was set to 200 eV, resulting in an energy resolution better than 0.6 eV. For all samples it was necessary to use an electron flood gun to stabilise the surface charge. Use of a flood gun shifts all spectral features to high kinetic energy. Photoelectron spectra were therefore charge calibrated using the weak C 1s contaminant peak which was assigned a binding energy of 285.0 eV. The spectrometer is calibrated regularly to set the Fermi edge of a silver reference sample at zero binding energy. Diffuse reflectance (DR) spectra were measured in the visible and near-ultraviolet (UV) region using a Perkin-Elmer Lambda 650 instrument equipped with a Praying-Mantis mirror construction.

X-ray absorption fine structure (XAFS) measurements were carried out at HASYLAB (DESY in Hamburg, Germany) on the beamlines C and X1 (Sn*K* edge 29200 eV) using a double-crystal Si(3 1 1) monochromator, which was detuned to 50% of maximum intensity to exclude higher harmonics in the X-ray beam. The spectra were recorded in the transmission mode at liquid nitrogen temperature. For the measurements the appropriate amount of each sample was pressed into self supporting pellets (13 mm diameter) and wrapped with Kapton tape. All the spectra were measured simultaneously with the reference spectrum of Sn foil placed between second and third ionisation chambers, so that the absolute energy calibration is performed. The spectra of Sn(II) and Sn(IV) oxides, which were used as references, were collected at the same conditions. All spectra were measured twice to ensure their reproducibility.

Analysis of the EXAFS spectra was performed with the software VIPER for Windows [22]. In the spectra of the absorption coefficient μ, a Victoreen polynomial was fitted to the pre-edge region for background subtraction. A smooth atomic background μ_0 was evaluated using a smoothing cubic spline. The Fourier analysis of the k^2-weighted experimental function $\chi = (\mu - \mu_0)/\mu_0$ was performed with a Kaiser window. The required scattering amplitudes and phase shifts were calculated by the ab initio FEFF8.10 code [23] for SnO_2 rutile-type tetragonal structure. The fitting was done in the *k*- and *r*-spaces. The shell radius *r*, coordination number *N*, Debye–Waller factor σ^2 and adjustable "muffin-tin zero" ΔE were determined as fitting parameters. The errors of the fitting parameters were found by decomposition of the statistical χ^2 function near its minimum, taking into account maximal pair correlations.

2.3. Photocatalytic characterisation

The photocatalytic activity was evaluated by monitoring the photodecomposition of an aqueous solution of methylene blue (MB) with a concentration of 10 ppm. TiO_2-based photocatalysts under UV irradiation have been shown to oxidise MB, with an almost complete mineralisation of carbon and of nitrogen and sulfur heteroatoms into CO_2, NH_4^+, NO_3^- and SO_4^{2-} respectively [24]. This method of assessing photocatalytic activity is a popular one for screening catalysts despite the possibility of direct photolytic degradation of the dye. To take account of this possibility the activity of all catalysts was always compared with that of pure anatase

Table 1
General physicochemical characteristics of samples used in this study.

Sample	Sn content % (w/w)[a] (at./nm^2)	Crystalline structure[b]	SSA[c] (m^2/g)
Anatase TiO_2	–	100% anatase	100
Sn(0.5)/TiO_2	1.04 (0.5)	100% anatase	98
Sn(1.0)/TiO_2	1.85 (1.0)	100% anatase	98
Sn(1.5)/TiO_2	2.60 (1.4)	100% anatase	97

[a] As determined from chemical analysis with ICP technique.
[b] As determined from XRD.
[c] As calculated from N_2 physisorption using B.E.T. method.

TiO_2. A 300 W Xe lamp was used as the radiation source using a cut-off filter for the removal of wavelength components shorter than 320 nm. In a typical photocatalytic experiment, a total of 42.5 mg of catalyst powder was added to 85 cm^3 of the methylene blue solution in a quartz tube. Prior to irradiation, the suspensions were magnetically stirred in the dark for 60 min to ensure the establishment of equilibrium coverage of the catalyst powder by the dye. At measured time intervals, aliquots of around 3 cm^3 were extracted and filtered through a 0.20 mm membrane filter to remove the catalyst particles. The filtrates were analysed by recording variations in the absorbance at 665 nm (the peak maximum in the absorption spectra) in a Perkin-Elmer Lambda 750S instrument. The percentage of methylene blue degradation was plotted against the time of irradiation to provide a quantitative indication of the activity of the catalyst.

A comparative analysis of the production rates of hydroxyl radicals (•OH) on the surface of the samples under UV irradiation was carried out by a fluorescence technique with terephthalic acid as a probe molecule. Terephthalic acid reacts rapidly with •OH to produce 2-hydroxyterephthalic acid, which is a highly fluorescent compound. The intensity of the fluorescence spectrum of 2-hydroxyterephthalic acid is proportional to the amount of •OH radicals formed in water [25]. This technique is commonly used for the photocatalytic characterisation of semiconductors in water [26,27]. In a typical photocatalytic experiment, a total of 42.5 mg of catalyst powder was added to 85 cm^3 of 3×10^{-3} M terephthalic acid solution in 1.5×10^{-2} M NaOH in a quartz tube. Prior to irradiation, the suspensions were magnetically stirred in the dark for 60 min. At measured time intervals, aliquots of around 3 cm^3 were extracted and filtered through a 0.20 mm membrane filter to remove the catalyst particles. The filtrates were analysed by recording the increase in the fluorescence emission at 425 nm (the peak maximum in the spectra) in a Fluorolog-3 from Horiba Jobin Yvon and plotted versus time.

3. Results and discussion

Table 1 summarises some physicochemical properties of the samples used in this study. Structural analysis of samples by X-ray diffraction and Raman spectroscopy showed that there is no development of secondary structures upon Sn loading, whereas analysis of nitrogen physisorption indicated that the specific surface area of anatase TiO_2 remains essentially unchanged.

3.1. Reduction profile of Sn(IV)-grafted TiO_2

Fig. 1 shows TPR profiles of pure and Sn-grafted anatase samples. The reduction profile of anatase TiO_2 shows that this sample is poorly reducible with an overall H_2 uptake of ~0.10 mmol H_2/g. It is possible however to distinguish two regions of H_2 consumption: one in the 430–650 °C temperature range, and a second one at temperatures higher than 750 °C. Based on previous literature, the first region of H_2 consumption may be assigned to TiO_2 surface reduction. In a study of the kinetics of TiO_2 reduction in H_2, Rekoske and Barteau [28] found that the reduction profile of TiO_2 at temperatures from 400 °C to 500 °C was best described by a scheme that includes only surface species or near surface species. Given the small value of H_2 uptake it is reasonable to expect that the reduction process of TiO_2 in these conditions is surface limited. We think therefore H_2 consumption at around 750 °C is due to further surface reduction in more stable TiO_2 surfaces.

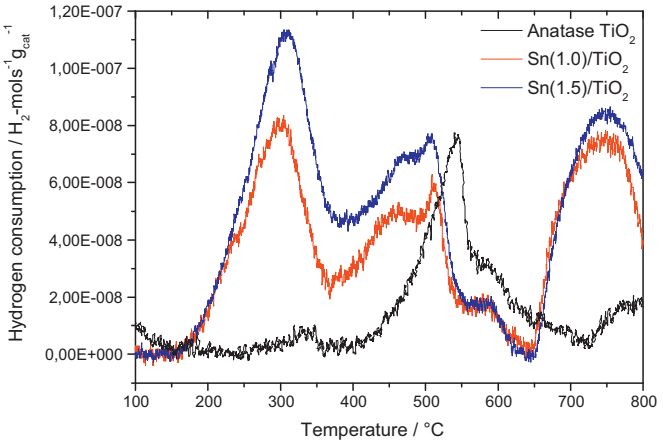

Fig. 1. Temperature-programmed reduction profiles of (a) pure and (b) Sn-grafted anatase TiO_2.

There is an increase in the overall H_2 consumption upon Sn-grafting, reaching ~0.31 mmol H_2/g for Sn(1.0)/TiO_2 and 0.42 mmol H_2/g for Sn(1.5)/TiO_2. It is interesting to notice that for all Sn-grafted samples the total H_2 consumption is about twice the total amount of tin in each sample (0.155 mmol Sn/g for Sn(1.0)/TiO_2 and 0.219 mmol Sn/g for Sn(1.5)/TiO_2), which matches a complete reduction of Sn(IV) to metallic Sn. Reduction to metallic Sn has been previously reported in studies of the reduction profile of SnO_2, which show that the reduction process normally involves a single asymmetric broad peak of hydrogen consumption centred at about 750 °C [29–31]. However, TPR profiles of all Sn-grafted TiO_2 samples, also shown in Fig. 1 indicate that a more complex reduction process occurs for these solids as at least three regions of hydrogen consumption can be clearly distinguished in the profiles. There is a high temperature H_2 consumption centred at around 750 °C similar to that in the TPR of SnO_2 which leads to the formation of metallic tin. There are also two further hydrogen consumption maxima centred at 280 °C and 490 °C. Sasikala et al. found a similar secondary hydrogen consumption centred at 290 °C on the TPR profile of high surface SnO_2 powders [32]. They also found this low temperature H_2 consumption was greatly decreased after sintering the sample, which led the authors to suggest it was associated to surface tin reduction of the material. According to our synthesis procedure, tin is expected to be present only at the surface of the solid, and therefore a similar low temperature process should take place in the reduction of our samples. We therefore assign low temperature H_2 consumptions to the reduction of Sn surface species with different Sn–O–Ti interactions, probably derived from difference in the coordination array on TiO_2 surfaces. Structural characterisation presented later in this paper shows Sn-grafted samples lack extended Sn coordination (Sn–O–Sn), and therefore such coordination should only have a minor contribution to the TPR of our samples.

We carried out a more detailed study on the reduction around the low temperature hydrogen consumption aiming to achieve a more thorough understanding of the surface reduction process that could lead to the formation of Sn(II) species. Based on the TPR profiles of studied samples, we performed reduction treatments in 5%H_2/Ar at 250–350 °C and carried out electronic and structural

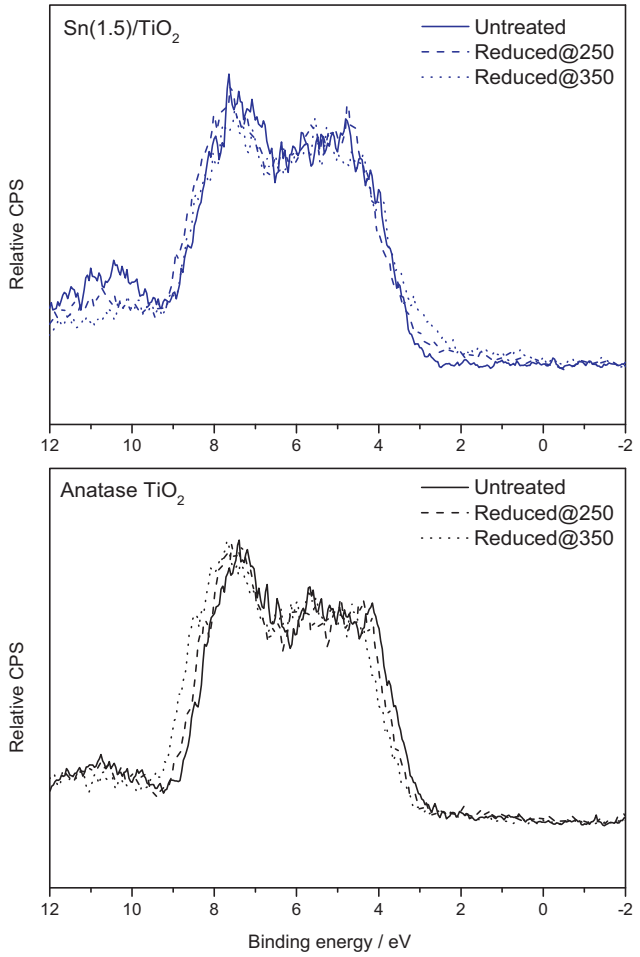

Fig. 2. Valence band photoelectron spectra of pure and Sn-grafted anatase TiO_2 and the effect of in situ reduction in 10 torr H_2 at temperatures up to 350 °C.

characterisation of samples before and after reduction. Results presented below clearly show the formation of surface Sn(II) and the concomitant effect on the photocatalytic efficiency.

3.1.1. *Effect of reduction on the electronic structure of Sn-doped anatase TiO_2*

3.1.1.1. X-ray photoelectron spectroscopy. Fig. 2 shows valence band photoemission spectra of anatase TiO_2 and Sn(1.5)/TiO_2 before and after *in situ* reduction in 10 torr of H_2 at temperatures up to 350 °C. Binding energies are referenced to the Fermi level of TiO_2 which is pinned close to the conduction band minimum (CBM) by donor states. Thus the binding energy of the valence band maximum (VBM) in spectra of TiO_2 corresponds to the band gap energy. As seen in the lower panel of Fig. 2, the spectrum of anatase TiO_2 has an onset of emission at about 3 eV, which is consistent with the band gap value for TiO_2. Upon reduction there is neither a change in the relative spectral intensity of anatase TiO_2 nor the appearance of new structures in the spectrum, which is consistent with the poor reducibility of TiO_2 discussed above. In the reduction of Sn(1.5)/TiO_2 however there is a clear increase in spectral intensity at the top of valence band maximum (VBM) upon reduction (upper panel of Fig. 2). A similar tailing of filled states at the top of the VBM has been observed in electron photoemission studies of reduced SnO_2 [33] as well as TiO_2 nominally doped with Sn(IV), and such states have been assigned to (O 2p–Sn 5s)* + Sn 5p hybrid states associated with Sn cations in the divalent state occupying surface sites, as discussed above. It is important to notice that the characteristic signal assigned to Ti(III)-derived surface states which appears at binding energies below 1 eV was not detected in any spectra. Also, core level XPS analysis (not shown) showed no signal associated to the presence of metallic Sn at the surface of reduced Sn-doped samples. This indicates that reduction of Sn-doped TiO_2 at temperatures up to 350 °C only involves the process Sn(IV) to Sn(II). Sn(II)-derived states at the top of the VBM of TiO_2 induce strong visible light absorption and give reduced samples a characteristic yellow colour. Although XPS of samples with lower Sn loading do not clearly show electronic states arising at the top of the valence band after reduction (not shown), they all present the characteristic yellowish colour (see UV/vis diffuse reflectance spectroscopy study below). We therefore think this is due to the low signal-to-noise ratio, which is characteristic of valence band XPS.

Table 2
Surface tin concentration.

Photocatalyst	Sn concentration, %Sn/(Ti + Sn) [a]	
	Calcined	Reduced at 250 °C
Sn(0.5)/TiO_2	3.3	
Sn(1.0)/TiO_2	5.5	6.6
Sn(1.5)/TiO_2	8.2	8.9

[a] Based on Ti 2p and Sn 3d core levels after sensitivity factor correction.

Table 2 shows results of quantitative surface chemical analysis based on core XPS levels after correction by sensitivity factors. It can be seen that surface Sn concentrations range from 3% to 9%, which is in a range of *bulk* concentrations studied in references cited in this work. It is important to notice that there is a small increase of the Sn surface concentration upon reduction. Such segregation might be related to the reduction of Sn(IV) ions incorporated in near surface Ti(IV) sites. As described in detail elsewhere, the internal electronic energy of Sn(II) ions in the solid state oxide is lowest when the cation occupies sites that lack inversion symmetry, such as surface sites. Therefore surface segregation of the reduced dopant cation lowers the surface energy of the solid, which provides the driving force of the process.

3.1.1.2. UV/vis diffuse reflectance spectroscopy. Diffuse reflectance spectra of anatase TiO_2 and Sn-grafted TiO_2 samples in the loading range studied are shown in Fig. 3a as plots of $\log(1/R)$ versus photon energy $h\nu$. There is no appreciable change of the anatase TiO_2 spectrum upon Sn-grafting. This observation contrasts with previous theoretical and experimental studies of Sn-doping in anatase TiO_2, which have found that Sn-doping in anatase TiO_2 always resulted in an increase of the value for the bulk bandgap [13,34]. However, provided diffuse reflectance spectroscopy is bulk sensitive technique, the overall Sn concentration of tin may be too low to produce an observable effect on the anatase spectrum. Reduction of Sn-grafted samples brings about an increase of the absorption in the visible region tailing up to a photon energy of about 2 eV. Such increase in spectral intensity in the visible region is consistent with the valence band XPS analysis shown above, and we assign it to (O 2p–Sn 5s)* + Sn 5p hybrid states associated with Sn cations in the divalent state occupying surface sites.

The stability of Sn(II) derived states under UV irradiation in air was gauged by the intensity of their absorption upon irradiation over extended time. Fig. 3b shows diffuse reflectance spectra of Sn(1.5)/TiO_2 reduced at 250 °C after UV irradiation for up to 5 h in air. It can be seen that there is a decrease of the intensity of the absorption after 1 h of irradiation; however further exposure up to 5 h causes only negligible changes in the absorption intensity of these states. This could be caused by a partial reoxidation of Sn(II) species which might compromise the stability of the photocatalysts prepared. However, in the study of the photocatalytic stability described later in this paper, it was found that the system remains active after ordinary storage and UV irradiation.

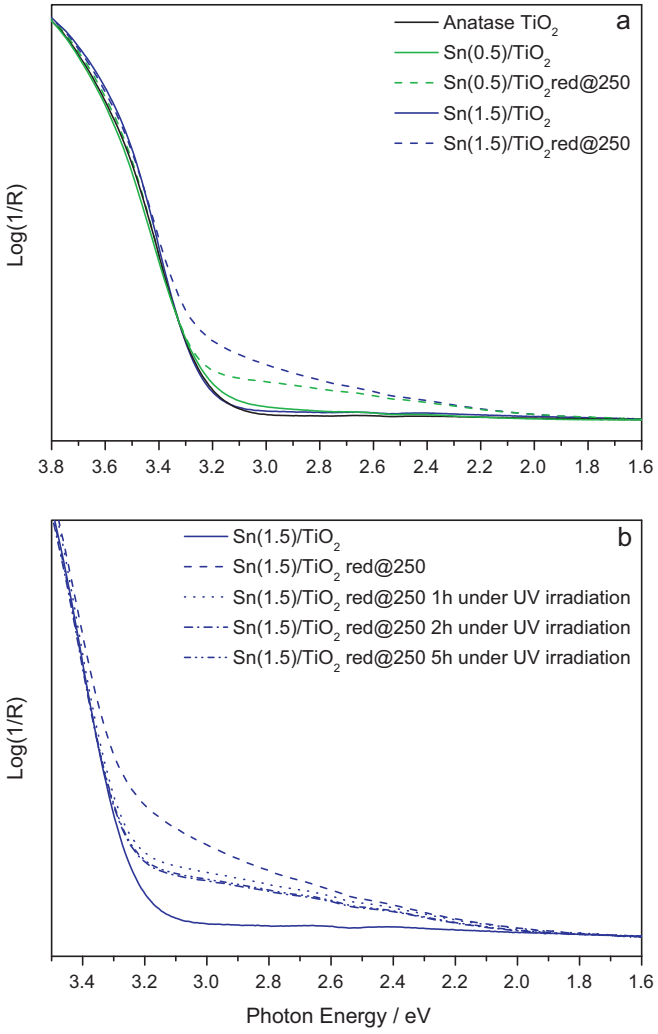

Fig. 3. (a) UV/vis diffuse reflectance spectra of anatase TiO_2 and Sn(x)/TiO_2 before and after reduction in 5%H_2 in argon at 250 °C. (b) UV/vis diffuse reflectance spectra of reduced Sn(1.5)/TiO_2 after UV irradiation in air. All spectra are presented in terms of log(1/R) versus photon energy.

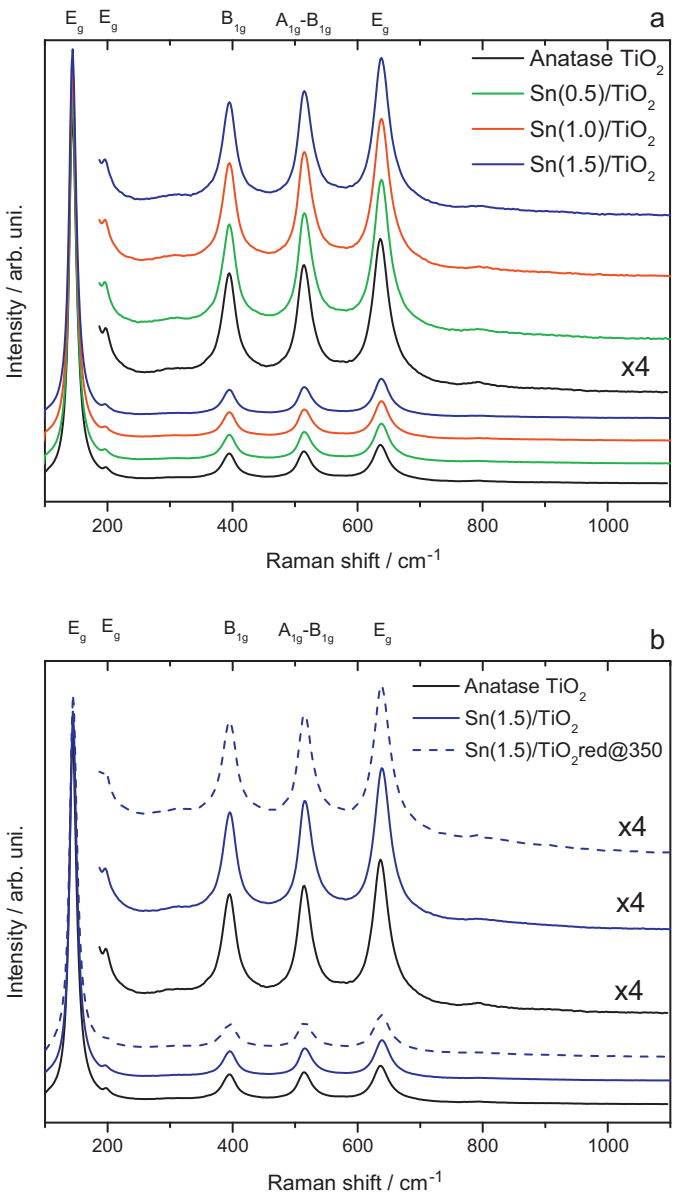

Fig. 4. (a) Raman spectra of anatase TiO_2 and Sn-grafted anatase in the loading range studied. (b) Raman spectra of anatase TiO_2 and 1.5Sn-grafted antase TiO_2 before and after reduction in 5%H_2 in argon at 350 °C.

3.1.2. *Structure of Sn-grafted anatase TiO_2 upon reduction*

3.1.2.1. Raman spectroscopy. Fig. 4 shows Raman spectra of anatase TiO_2 and Sn-grafted anatase TiO_2 in the loading range studied. Details of the Raman spectra of the sample with highest Sn loading are also shown before and after reduction in 5%H_2 in argon at 350 °C. A clear set of bands characteristic of a single anatase phase was observed for all samples. Anatase TiO_2 belongs to the space group D_{4h}^{19}(I4/amd) and displays six Raman active fundamental vibration modes, $A_{1g} + 2B_{1g} + 3E_g$. Raman spectra of the undoped TiO_2 sample showed peaks at 144 cm^{-1}, 197 cm^{-1} and 639 cm^{-1} which are assigned in accordance with the literature to E_g vibrations, as well as peaks at 399 cm^{-1} and 516 cm^{-1} which correspond to B_{1g} and an overlap of A_{1g} and the second B_{1g} vibration modes, respectively [35]. Weak features near 320 cm^{-1}, 695 cm^{-1} and 796 cm^{-1} are also characteristic of the Raman spectrum of anatase and have been assigned to combination bands.

As seen in Fig. 4, neither Sn(IV) grafting nor the subsequent reduction of the sample cause the appearance of any additional band in the Raman spectrum of bare anatase TiO_2 even for the sample with the highest loading of tin, Sn(1.5)/TiO_2. This indicates that neither Sn loading nor the subsequent reduction process bring about any major changes in the bulk structure of the sample. No agglomeration of tin species resulting in the formation of crystalline SnO_2 during the grafting process can be detected by Raman spectroscopy. Similarly, it was verified that the Raman spectra of samples recovered after photocatalytic tests only consisted of the set of bands characteristic of anatase TiO_2.

3.1.2.2. Extended X-ray absorption fine structure. The sample with highest Sn loading and therefore the most likely to present SnO_2 agglomeration was subject of a detailed XAFS experiment. Fig. 5 shows Fourier transformed Sn K-edge EXAFS for Sn(1.5)/TiO_2 before and after reduction in 5%H_2 in argon at 250 °C. The figure also shows Sn K-edge EXAFS for SnO_2 and SnO for reference. All distances are uncorrected for the phase shifts. The Fourier transformed EXAFS spectrum of SnO_2 reference shows two intense features with maxima at about 1.6 Å and 3.4 Å, followed by five features in the 4–8 Å range. The two major features have been well fitted with a model that includes a first six-oxygen coordination shell

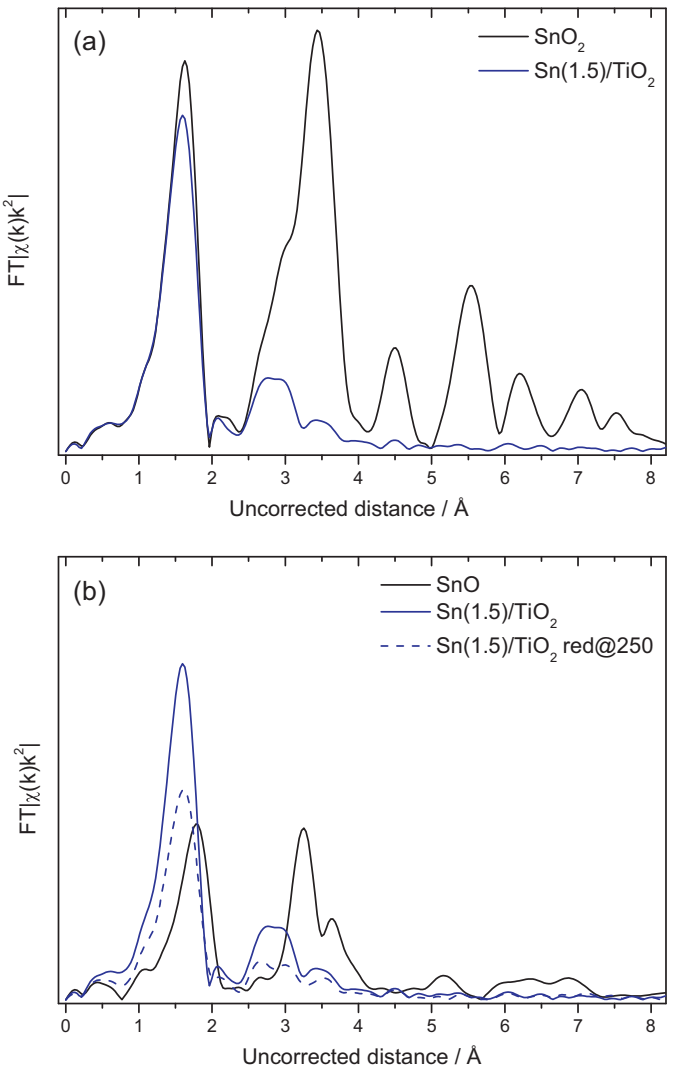

Fig. 5. (a) Sn K-edge spectra for Sn(1.5)/TiO_2 and a reference SnO_2, (b) Sn K-edge spectra for Sn(1.5)/TiO_2 before and after reduction in 5%H_2 in argon at 250 °C along with a reference SnO.

at 2.06 ± 0.02 Å, related to the first peak, and secondary two-tin and eight-tin coordination shells at 3.18 ± 0.02 Å and 3.71 ± 0.02 Å, respectively [36,37]. A second four-oxygen shell at 3.594 Å, according to crystallographic data, makes only a minor contribution to the EXAFS as this is a shell of weakly backscattering atoms [37] compared with heavy Sn atoms. Peaks at $R > 4$ Å are related to tin shells located at longer distances in the crystalline reference [36].

Fig. 5a shows the Sn K-edge Fourier transformed EXAFS spectra of Sn(1.5)/TiO_2 and bulk SnO_2 (reference). Except for the peak related to the first oxygen shell, all features appear with much lower intensity or are not observed at all. The small feature in the 2.5–4 Å range may emerge from the interaction with secondary oxygen and titanium shells. This indicates that the local structure of Sn atoms lacks long range order and therefore confirms the single site nature of Sn atoms in grafted samples. This observation is consistent with the absence of evolution of any secondary crystalline phase upon grafting as determined by XRD and Raman spectroscopy analysis. Single isolated tin atoms on TiO_2 surfaces has been previously achieved by Gu et al. using tetramethyltin as tin precursor [38].

Fig. 5b shows Sn K-edge Fourier transformed EXAFS spectra of Sn(1.5)/TiO_2 before and after reduction. There is an overall decrease of the spectrum intensity upon reduction which could be related to a decrease in oxygen coordination number. Table 3 shows the distance and coordination number of the first oxygen shell derived from curve fits to the EXAFS spectra. As shown there is a decrease of the average coordination number of the first oxygen shell from 5.81 to 4.27 that comes along with a slight expansion of the radius of that first shell. In accordance with valence band XPS analysis, this shows that there is a net reduction of Sn(IV). However, the spectrum of this reduced species does not resemble that of bulk SnO (also shown in Fig. 5b as reference) which indicates that no cluster is formed during the reduction process.

Table 3
Information derived from curve fits to the EXAFS spectra.

Sample	R (Å)	Coordination number
SnO_2	2.05 ± 0.01	5.85 ± 0.29
SnO	2.22 ± 0.02	4.12 ± 0.18
Sn(1.5)/TiO_2	2.05 ± 0.01	5.81 ± 0.21
Sn(1.5)/TiO_2 red@250	2.07 ± 0.01	4.27 ± 0.13

Structural characterisation with EXAFS indicated the grafting process and subsequent reduction leads to the formation of isolated species in different oxidation states chemically attached to the surfaces of TiO_2. Therefore the system can be considered as a doping restricted to the surface rather than a semiconductor coupling system.

3.2. Effect of surface Sn(II) on the photocatalytic oxidation of dyes

Results of the photocatalytic activity characterisation as gauged by means of photocatalytic degradation of methylene blue are shown in Fig. 6. Fig. 6a shows a comparative study of the activity under irradiation >320 nm for anatase TiO_2 and Sn-grafted samples, and the effect of the reduction at 250 °C. The photocatalytic activity of anatase TiO_2 was found to decrease upon Sn-grafting. Treatment of bare anatase TiO_2 in H_2 at 250 °C also led to a decrease in photocatalytic activity. However, reduction of Sn-grafted anatase TiO_2 in the same conditions resulted in a notable increase of photocatalytic activity to almost twice that of anatase TiO_2 before reduction. In a study done for selected samples it was shown that except for the case of reduced bare titania, there are only negligible changes of the dye adsorption on the surface of the catalysts upon reduction (see Fig. 7), which rules out this property as a factor to explain the increased photocatalytic activity of reduced Sn-grafted samples.

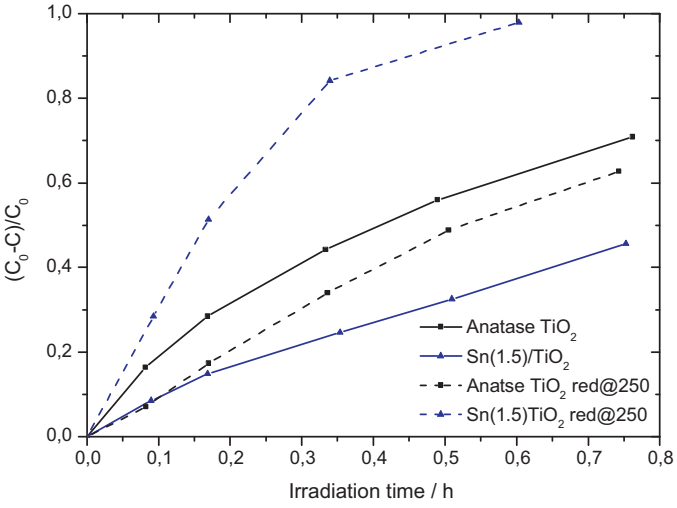

Fig. 6. Photocatalytic activity towards methylene blue degradation of TiO_2 and Sn(1.5)/TiO_2 before and after reduction in 5%H_2 at 250 °C. Irradiation source: 300 W Xe lamp with 320 nm cutoff filter.

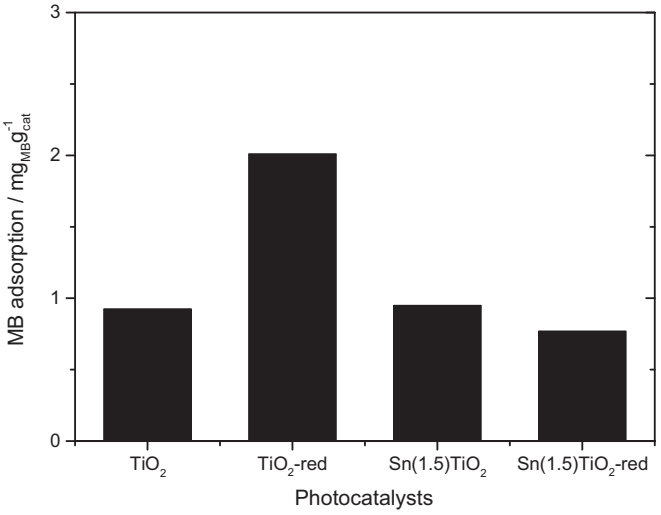

Fig. 7. Methylene blue adsorption on selected photocatalysts after 60 min stirring in a 10 ppm solution.

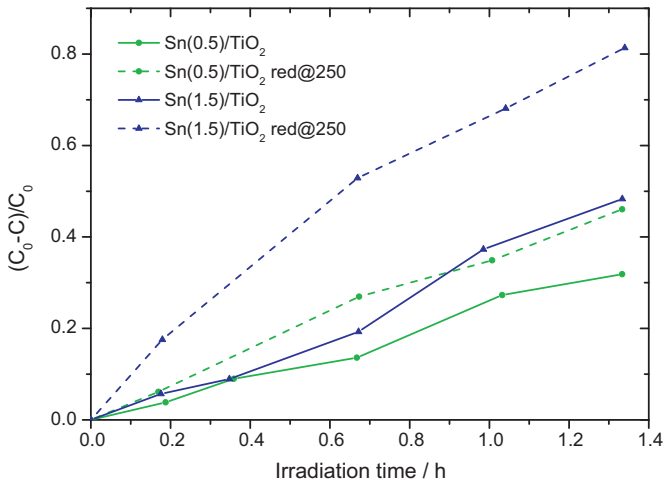

Fig. 8. Photocatalytic activity towards methylene blue degradation of Sn(0.5)/TiO_2 and Sn(1.5)/TiO_2 before and after reduction in 5%H_2 at 250 °C. Irradiation source: 150 W Xe lamp with 320 nm cutoff filter.

On the other hand, the increase of the photocatalytic activity does parallel the pronounced increase in the intensity of the tail of visible region absorption that is associated with Sn^{2+} ions at surface and grain boundary interfaces. Sn(II)-derived surface states may bring about an increment of the photocatalytic activity by a combined effect of an extended light absorption and the surface trapping of holes produced under irradiation. Charge trapping could be considered beneficial if it localises charge carriers at important electron transfer sites on TiO_2 surfaces or if it promotes charge carrier separation [40]. In studies of kinetics of TiO_2-based photocatalytic oxidation in water, two non-selective *oxidising agents* were identified to be produced under irradiation, *valence band holes* and •*OH radicals*. Both increased recombination time of charge carriers and surface localisation of trapped holes would lead to an increased formation rate of the oxidising agents involved in photocatalytic degradation of methylene blue. Although trapped holes have a reduction potential less positive than those located in the main valence band, they still might act as oxidising agents provided the trapping energy is not too high. Increased photocatalytic activity upon reduction in H_2/Ar at 250 °C was observed for all Sn-grafted samples; however, the effect was strongest in the sample with the highest Sn loading, Sn(1.5)/TiO_2 (Fig. 8).

Fig. 9 shows results of a study concerning the stability of the reduced samples. Fig. 9a shows the photocatalytic activity of Sn(1.5)/TiO_2 reduced in H_2 at 250 °C for methylene blue degradation, measured right after reduction and after two weeks of storage in ordinary conditions (in air at room temperature). It can be seen that there is no major effect on the high activity of the sample which shows these catalysts are stable in oxidising atmosphere. On the other hand, Fig. 9b shows the photocatalytic activity of Sn(1.5)/TiO_2 reduced in H_2 at 250 °C after pre-irradiation under UV light in water compared with the photocatalytic activity of the samples with no pre-irradiation. It is important to consider that this experiment was carried out in a different setup that included a less intense Xe lamp (150 W) and therefore the degradation rate is in general lower than that in Fig. 7a. It can be seen that there is no decrease of the photocatalytic activity upon UV irradiation of the sample previous to the photocatalytic test, but instead a slight increase of the photocatalytic activity of the sample is observed. Further stability tests that include the reusability of the reduced photocatalyst are shown in Fig. 9c. The conversion versus time plots for a photocatalyst recovered from a first 80-min test is compared with that of fresh photocatalyst. As shown, the material keeps its high activity throughout a second run, and an even higher activity is observed. The reasons for this increase in activity are not clear yet, but since structural changes can be ruled out, the observed increase in activity might be related to a surface activation during the photocatalytic process. This hypothesis is subject of current investigation and will be further discussed in a future paper. However, these stability tests certainly suggest that partial reoxidation of reduced Sn-grafted samples that might take place upon UV irradiation in air does not seem to detrimentally affect the photocatalytic activity of the samples dispersed in aqueous solution.

Fig. 10 shows results for the quantification of surface •OH radicals generation upon UV illumination. Fig. 10a shows changes with illumination time of the fluorescence emission spectra of a 3×10^{-3} M terephthalic acid solution in 1.5×10^{-2} M NaOH containing a suspension of anatase TiO_2. The excitation radiation was fixed at 315 nm. It can be seen that the characteristic spectrum of 2-hydroxyterephthalic acid (HTA) continuously increases in intensity. Such increase could not be detected in absence of either UV illumination or a photocatalyst, which confirms that HTA is formed by chemical reactions of terephthalic acid with •OH formed on the TiO_2/water interface via photocatalytic reactions previously found [27,39]. Provided •OH are highly reactive, formation of HTA can be directly related to the generation of •OH on the surface of the catalysts [25]. •OH radicals can be formed in a TiO_2/water system either by oxidation of water by holes

$$H_2O + h^+ \rightarrow H^+ + {}^\bullet OH \quad (1)$$

or by transient formation of hydroperoxide radicals

$$O_{2(g)} + e^- \rightarrow O_2^{\bullet -} \quad (2)$$

$$O_2^{\bullet -} + H^+ \rightarrow HO_2^\bullet \quad (3)$$

$$2\,HO_2^\bullet \rightarrow H_2O_2 + O_2 \quad (4)$$

$$H_2O_2 + e^- \rightarrow OH^- + {}^\bullet OH \quad (5)$$

However, it is important to mention that under the conditions in which the TA hydroxylation test is performed, the only feasible pathway for the generation of •OH radical is an oxidative attack of H_2O and/or ^-OH by holes generated in the valence band under light irradiation. The alternative route, formation of hydroperoxide radical, is inhibited by the alkaline condition under which the test is performed.

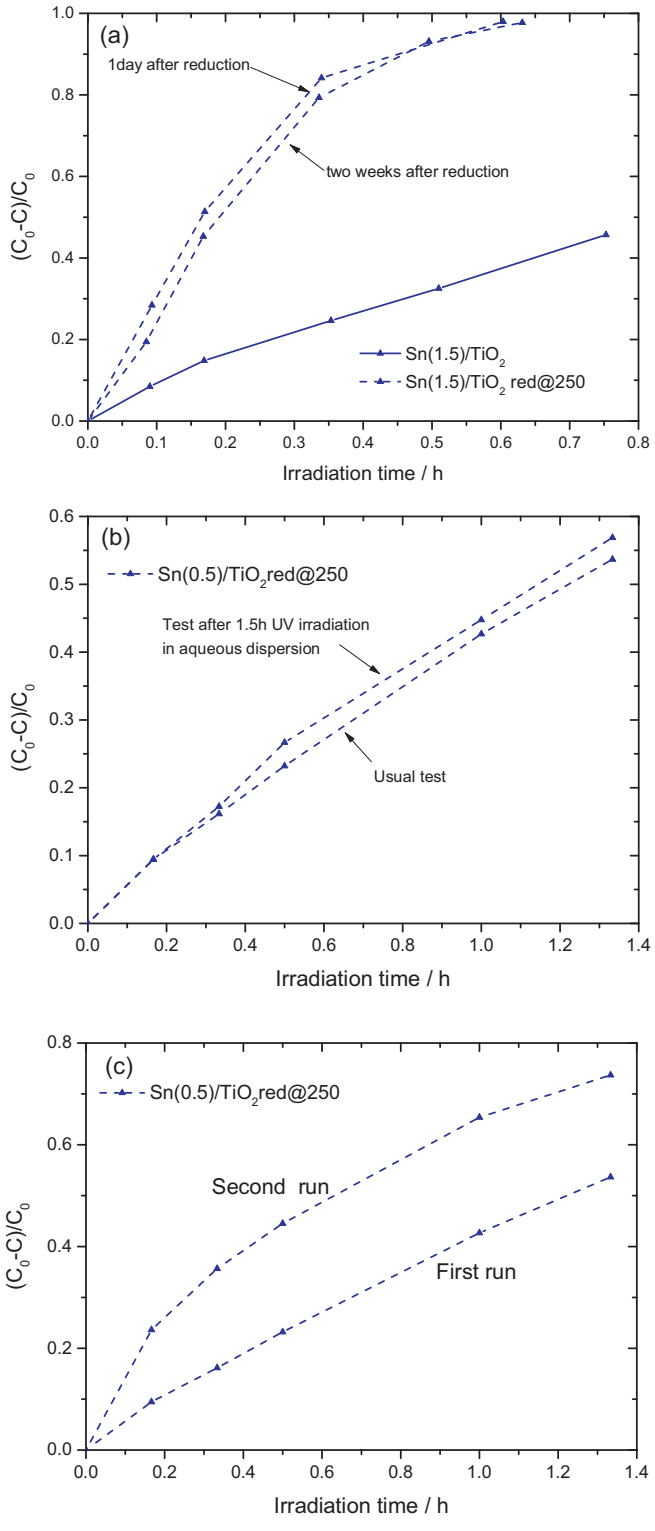

Fig. 9. (a) Photocatalytic activity towards methylene blue degradation of $Sn(1.5)/TiO_2$ reduced in H_2 at 250 °C after different time of ordinary storage. Irradiation source: 300 W Xe lamp with 320 nm cutoff filter, (b) photocatalytic activity towards methylene blue degradation of $Sn(1.5)/TiO_2$ reduced in H_2 at 250 °C after pre-irradiation under UV light compared with the photocatalytic activity of the sample with no pre-irradiation. Irradiation source: 150 W Xe lamp with 320 nm cutoff filter, and (c) photocatalytic activity towards methylene blue degradation of $Sn(1.5)/TiO_2$ reduced in H_2 at 250 °C recovered from an 80-min test compared with the photocatalytic activity of the fresh sample. Irradiation source: 150 W Xe lamp with 320 nm cutoff filter.

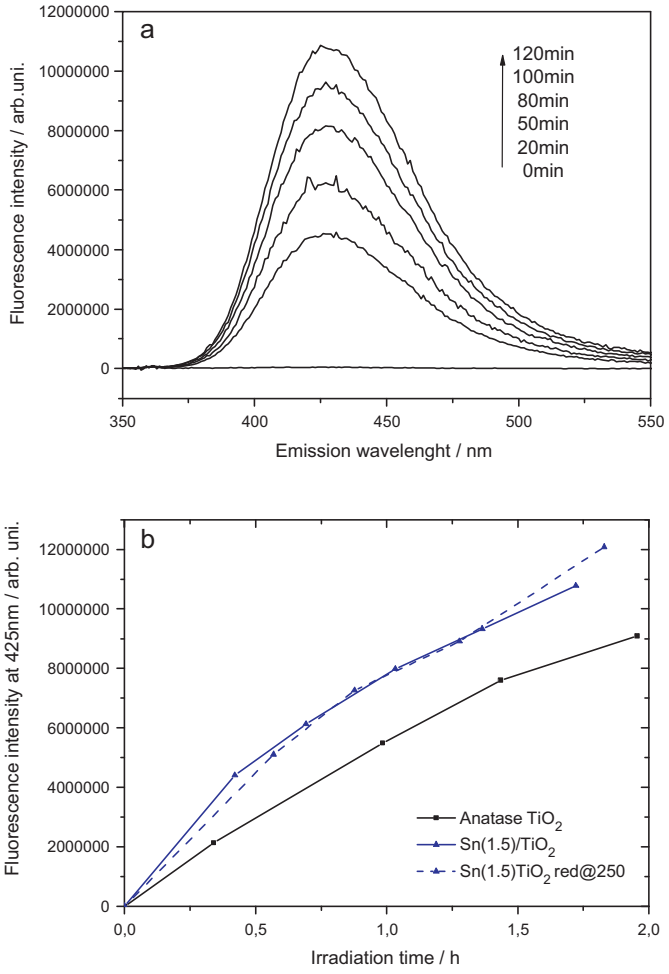

Fig. 10. (a) Fluorescence spectra changes observed in a 1.5×10^{-3} M basic solution of terephthalic acid during irradiation with >320 nm in presence of anatase TiO_2 sample. (b) Plots of the fluorescence at 425 nm versus irradiation time for terephthalic acid solution in presence of bare TiO_2 and $Sn(1.5)/TiO_2$ before and after reduction. Spectra were recorded using an excitation radiation fixed at 315 nm.

Fig. 10b shows plots of the spectra intensity at 425 nm versus irradiation time for anatase TiO_2 and $Sn(1.5)/TiO_2$ before and after reduction in H_2 at 250 °C. It can be seen that there is an increase in the •OH generation rate upon Sn grafting. Although differences in water adsorption might influence the •OH generation rate, water adsorption experiments showed that neither Sn-doping nor subsequent reduction treatments bring about mayor changes of the water adsorption on the samples (not shown). However, Sn(II) surface states created upon reduction do not seem to alter the rate of •OH formation. This may be related to a lower oxidising potential of holes trapped in Sn(II)-related surface state compared with holes in the main valence band. The standard reduction potential of the $^{\bullet}OH/H_2O$ pair is +2.38 V which is close to that of the valence band potential (~3 V). Provided Sn(II)-related surface states extend up to 1 eV from the VBM (see electronic structure characterisation above), holes trapped in these states may not have enough oxidising power to promote the formation of •OH radicals. Therefore, only those holes in the main valence band could oxidise adsorbed water to produce •OH radical similarly to the unreduced grafted samples. The oxidising power of both reduced and unreduced grafted anatase TiO_2 samples may be higher than that of bare anatase TiO_2 due to a shift of the VBM towards higher potentials upon Sn-grafting. As mentioned above, experimental and theoretical research on anatase $Sn_xTi_{1-x}O_2$ shows that there is monotonic increase of the anatase TiO_2 band gap upon tin

doping, which is due to shift of the VBM towards higher binding energy.

It is to be noted that results of •OH generation rate do not parallel those for degradation of methylene blue described above. This probably means that the reaction of degradation of methylene blue mainly proceeds via a direct oxidation by holes in the TiO_2 VB, as well as by holes trapped in Sn(II)-related surface states, and oxidative attack by •OH radicals generated from transient formation of hydroperoxide radicals. In their study on the degradation pathway of methylene blue on TiO_2/UV systems, Houas et al. propose a mechanism that includes a first step of methylene blue adsorption followed by multiple attacks by either holes produced under excitation or •OH radicals [24].

It is to be pointed out, however, that recently Tada et al. have shown theoretically that during photocatalysis by TiO_2 most organic molecules can be directly oxidised by surface trapped holes, while the oxidation of some organic molecules with low HOMO energies progresses mainly through indirect oxidation by •OH radicals [41]. It is therefore very important to carry out detailed studies of the mechanism of surface charge trapping in order to find systems in which the trapping energy is optimum for a maximum photocatalytic performance. We are at the moment working on expanding the concept of surface doping with post-transitional metals in the $N-2$ oxidation state to other systems.

4. Conclusions

Sn(IV) was successfully grafted on anatase TiO_2 by a relatively simple procedure using Sn(IV) *tert*-butoxide as the source of Sn. Structural characterisation showed that Sn species are most likely to be isolated, and the system can therefore be considered as TiO_2 surface doping with Sn. Grafting Sn(IV) on TiO_2 leads to formation of Sn-derived states restricted to the surface of the material, and it is possible to generate Sn(II) surface states by controlled reduction as there is a preferential reduction of surface tin over titanium. The Sn(II) surface states in doped TiO_2 lie above the top of the main valence band and can therefore act as surface trapping sites for holes produced under photoexcitation. These states of reduced Sn seem to be stable in oxidising conditions of reactions and storage.

The generation of Sn(II) surface states greatly enhances the photocatalytic efficiency of bare anatase TiO_2 for the degradation of methylene blue which may be extended to other dyes. Enhanced photocatalytic efficiency can be attributed to the larger number of photogenerated holes present at the surface of the material as Sn(II) surfaces states act as hole trapper sites. Although our results suggest trapped holes at the surface may lose their oxidising power to promote generation of •OH radicals, they may still be involved in direct surface oxidation. At the same time, surface charge trapping may promote the transient formation of hydroperoxide radical by increasing the electron/hole recombination time.

Acknowledgements

This work was funded by the German Ministry of Education and Research (BMBF) within the scope of the funding program "Technologies for Sustainability and Climate Protection - Chemical Processes and Use of CO_2".

References

[1] M. Ni, M.K. Leung, D.Y. Leung, K. Sumathy, Renewable and Sustainable Energy Reviews 11 (2007) 401–425.
[2] R. Asahi, Science 293 (2001) 269–271.
[3] S. Livraghi, M.C. Paganini, E. Giamello, A. Selloni, C. Di Valentin, G. Pacchioni, Journal of the American Chemical Society 128 (2006) 15666–15671.
[4] W. Choi, A. Termin, M.R. Hoffmann, Journal of Physical Chemistry 98 (1994) 13669–13679.
[5] J.H. Clark, M.S. Dyer, R.G. Palgrave, C.P. Ireland, J.R. Darwent, J.B. Claridge, et al., Journal of the American Chemical Society (2010) 1016–1032.
[6] T. Kutty, M. Avudaithai, Chemical Physics Letters 163 (1989) 93–97.
[7] F. Sayilkan, M. Asilturk, P. Tatar, N. Kiraz, S. Sener, E. Arpac, et al., Materials Research Bulletin 43 (2008) 127–134.
[8] Y. Cao, W. Yang, W. Zhang, G. Liu, P. Yue, New Journal of Chemistry 28 (2004) 218–222.
[9] F. Fresno, J.M. Coronado, D. Tudela, J. Soria, Applied Catalysis B: Environmental 55 (2005) 159–167.
[10] J. Lin, J.C. Yu, D. Lo, S. Lam, Journal of Catalysis 183 (1999) 368–372.
[11] T. Hirata, K. Ishioka, M. Kitajima, H. Doi, Physical Review B 53 (1996) 8442–8448.
[12] H. Uchiyama, H. Imai, Chemical Communications (2005) 6014–6016.
[13] Y. Zhao, J. Liu, L. Shi, S. Yuan, J. Fang, Z. Wang, et al., Applied Catalysis B: Environmental 103 (2011) 436–443.
[14] Y. Zhao, J. Liu, L. Shi, S. Yuan, J. Fang, Z. Wang, et al., Applied Catalysis B: Environmental 100 (2010) 68–76.
[15] D. Payne, R. Egdell, A. Walsh, G. Watson, J. Guo, P.-A. Glans, et al., Physical Review Letters 96 (2006) 157403.
[16] A. Walsh, D.J. Payne, R.G. Egdell, G.W. Watson, Chemical Society Reviews 40 (2011) 4455–4463.
[17] A. Walsh, G. Watson, Physical Review B 70 (2004) 235114.
[18] M.H. Harunsani, F.E. Oropeza, R.G. Palgrave, R.G. Egdell, Chemistry of Materials 22 (2010) 1551–1558.
[19] F.E. Oropeza, B. Davies, R.G. Palgrave, R.G. Egdell, Physical Chemistry Chemical Physics 13 (2011) 7882–7891.
[20] V.B.R. Boppana, R.F. Lobo, Journal of Catalysis 281 (2011) 156–168.
[21] J. Strunk, W.C. Vining, A.T. Bell, Journal of Physical Chemistry C 114 (2010) 16937–16945.
[22] K.V. Klementev, Journal of Physics D: Applied Physics 34 (2001) 209–217.
[23] A.L. Ankudinov, J.J. Rehr, S.D. Conradson, Physical Review B 58 (1998) 7565–7576.
[24] A. Houas, H. Lachheb, M. Ksibi, E. Elaloui, C. Guillard, J.M. Herrmann, Applied Catalysis B: Environmental 31 (2001) 145–157.
[25] K.-i. Ishibashi, A. Fujishima, T. Watanabe, K. Hashimoto, Electrochemistry Communications 2 (2000) 207–210.
[26] D. Bekermann, A. Gasparotto, D. Barreca, A. Devi, R.A. Fischer, M. Kete, et al., Chemistry: A European Journal 11 (2010) 2337–2340.
[27] J. Yu, W. Wang, B. Cheng, B.-L. Su, Journal of Physical Chemistry C 113 (2009) 6743–6750.
[28] J.E. Rekoske, M.A. Barteau, Journal of Physical Chemistry B 101 (1997) 1113–1124.
[29] P. Park, Journal of Catalysis 184 (1999) 440–454.
[30] R. Sasikala, S.K. Kulshreshtha, Journal of Thermal Analysis and Calorimetry 78 (2004) 723–729.
[31] X. Wang, Y.C. Xie, Catalysis Letters 75 (2001) 73–80.
[32] R. Sasikala, N. Gupta, S. Kulshreshtha, Catalysis Letters 71 (2001) 69–73.
[33] M. Batzil, K. Katsiev, J. Burst, Y. Losovyj, W. Bergermayer, I. Tanaka, et al., Journal of Physics and Chemistry of Solids 67 (2006) 1923–1929.
[34] R. Long, Y. Dai, B. Huang, Journal of Physical Chemistry C 113 (2009) 650–653.
[35] T. Ohsaka, F. Izumi, Y. Fujiki, Journal of Raman Spectroscopy 7 (1978) 321–324.
[36] G.E.S. Brito, V. Briois, S.H. Pulcinelli, C.V. Santilli, Journal of Sol-Gel Science Technology 8 (1997) 269–274.
[37] S.R. Davis, A.V. Chadwick, J.D. Wright, Journal of Physical Chemistry B 101 (1997) 9901–9908.
[38] Q. Gu, J. Long, Y. Zhou, R. Yuan, H. Lin, X. Wang, Journal of Catalysis 289 (2012) 88–99.
[39] M. Zhou, J. Zhang, B. Cheng, H. Yu, International Journal of Photoenergy 2012 (2012) 532843.
[40] M.A. Henderson, Surface Science Reports 66 (2011) 185–297.
[41] H. Tada, Q. Jin, H. Kobayashi, ChemPhysChem 13 (2012) 3457–3461.